Supporting Information

Graphene quantum dot surface ligand and Co and Pt double doping engineering Co/Co_3O_4 nanozyme superior to horseradish peroxidase and choline oxidase for efficient degradation of Rhodamine B without activator

Li Nana, Li Ruiyi, Li Zaijun[*] and Liu Xiaohao

Key Laboratory of Synthetic and Biological Colloids, Ministry of Education, School of Chemical and Material Engineering, School of Life Sciences and Health Engineering, Jiangnan University, Wuxi 214122, China

[*]Corresponding author: Tel.:13912371144. E-mail address: zaijunli@jiangnan.edu.cn (Li ZJ)

1. Experimental Section

1.1. Materials and reagents

Citric acid, tryptophan, glutamate, cobalt chloride, sodium acetate, acetic acid, chloroplatinic acid hexahydrate ($H_2PtCl_6·6H_2O$), hydrogen peroxide (H_2O_2), rhodamine B and other reagents employed were all of the highest analytical grade or quality reagents purchased from Shanghai Chemical Company (Shanghai, China). 3,3',5,5'-tetramethylbenzidine (TMB) was purchased from Sigma-Aldrich (Mainland, China). Acetate buffer (0.2 M, pH 3.5) was prepared by the laboratory. Ultrapure water (18.2 MΩ cm) purified from a Milli-Q purification system was used throughout the experiment.

1.2. Apparatus

Transmission electron microscope (TEM) images were conducted on Tecnai F20 microscope at 200 keV (FEI, America). X-ray photoelectron spectroscopy (XPS) measurement was performed using a Thermo Scientific K-Alpha spectrometer with monochromated Al Kα radiation (Thermo Scientific, America). X-ray diffraction (XRD) pattern was measured on X-ray D8 Advance Instrument operated at 40 kV and 20 mA, using Cu-Kα radiation source with λ=0.15406 nm (Bruker AXS, Germany). Raman measurement was carried out using InVia laser micro-confocal Raman Spectrometer (Renishaw, England). Infrared spectra (IR) were recorded on a Nicolet FT-IR 6700 spectrometer (Thermo Fisher Scientific, America). UV-visible spectra were recorded on UV-2700 spectrometer (Shimadzu, Japan). Electrochemical testing was conducted on CHI 660D (Chenhua, shanghai). UV-diffuse reflectance spectra were collected by a UV–vis–NIR spectrometer (Hitachi UV-3600 plus) with $BaSO_4$ as the background. Electron paramagnetic resonance (EPR) spectra were measured at room temperature using the Bruker EMX PLUS spectrometer. Total organic carbon (TOC) tests were performed by Rhodamine B degraded solution (10 mL) by a TOC analyzer (Shimadzu, TOC-VCPH, Japan).

1.3. EW-GQD preparation

Mixture of citric acid (2 g), glutamate (1.4 g) and tryptophan (0.97 g) were dissolved in 50 mL of ultrapure water. Then, it was heated at 80°C under stirring until free water was removed and at 170°C for 3 h. The collected EW-GQD crude was dissolved in ultrapure water to form a 100 mg mL^{-1} EW-GQD solution. To obtain EW-GQD, the solution was orderly treated by filtering, dialysis with 3000 Da and freeze-drying[1].

1.4. Steady-state dynamic parameter measurement

H_2O_2 and TMB were used as substrate to measure the steady-state dynamic parameters of Pt/Co/Co_3O_4/EW-GQD as peroxidas-like nanozyme, respectively[1]. When H_2O_2 was used as the substrate, a series of reaction solutions were prepared by mixing 100 μL of 1.0 mM TMB with 750 μL of 0.2 M acetate buffer solution (pH 3.5) and 100 μL of different concentration of H_2O_2 solution. After 50 μL of 1.0 mg mL^{-1} Pt/Co/Co_3O_4/EW-GQD dispersion was injected into the above reaction solution, the absorbances at 652 nm was monitored by spectrophotometer. When TMB was used as substrate, a series of reaction solutions were prepared by mixing 100 μL of 100 mM H_2O_2, 750 μL of 0.2 M acetate buffer solution (pH 3.5) and 100 μL of different concentration of TMB solution. After 50 μL of 1.0 mg mL^{-1} Pt/Co/Co_3O_4/EW-GQD dispersion was injected into the above reaction solution, its absorbances at 652 nm was monitored by spectrophotometer.

TMB was used as the substrate to measure the steady-state dynamic parameters of Pt/Co/Co_3O_4/EW-GQD as oxidase-like nanozyme. A series of reaction solutions were prepared by mixing 850 μL of 0.2 M acetate buffer solution (pH 3.5) and 100 μL of different concentration of TMB solution. After 50 μL of 1.0 mg mL^{-1} Pt/Co/Co_3O_4/EW-GQD dispersion was injected into the above reaction solution, its absorbances at 652 nm was monitored by spectrophotometer.

The steady-state dynamic parameters were calcuated by Lineweaver-Burk equation (1):

$$\frac{1}{V} = \frac{K_M}{V_{max}} \times \frac{1}{[S]} + \frac{1}{V_{max}} \qquad (1)$$

where V, V_{max}, [S] and K_M present the initial reaction rate, maximum reaction rate, substrate concentration and Michaelis-Menten constant of steady-state dynamic process.

1.5. Enzyme activity calculation

Specific activity of $Pt/Co/Co_3O_4$/EW-GQD nanozyme was calculated by the equation (2)[2]:

$$b_{nanozyme}=V/(\varepsilon \times L)\times(\Delta A/\Delta t) \qquad (2)$$

where, $b_{nanozyme}$ (U), V, ε, L and ΔA/Δt present the activity of nanozyme, total volume of a reaction system (1000 μL), molar absorption coefficient of TMB (39000 M^{-1} cm^{-1}), optical length of cell, and change rate of the absorbance at 652 nm. The specific activity ($a_{nanozyme}$, U mg^{-1}) of nanozyme was calculated by using equation (3)[2]:

$$a_{nanozyme}=b_{nanozyme}/[m] \qquad (3)$$

where, [m] presents mass of nanozyme.

1.6. DFT calculation

The reaction mechanism of oxidase and peroxidase-like $Pt/Co/Co_3O_4$/EW-GQD was studied by first principles calculation (DFT) method[3,4]. The generalized gradient approximation (GGA) of PBE functional was used to deal with variation-correlation interactions[5]. A double numerical (DN) base set is used for geometric optimization and total energy calculation. The k-point in the Brillouin zone is set to 2×2×1 mesh using the Monkhorst-Pack grid. The vacuum spacing perpendicular to the direction of the structural plane is 15 Å to avoid interaction between adjacent molecules. The convergence tolerance of SCF is 1.0×10^{-5} Ha.

The geometrically optimized energy and maximum force are 1.0×10^{-5} Ha and 0.004 Ha $Å^{-1}$, respectively. The crystal structures of the (2×2×1) Co_3O_4 (220) surface obtained from the Materials Project online service (ID: mp-18748) was built to represent the catalytic surfaces of catalyst. And graphene is obtained by supercell (3×3) the crystal surface of graphite (001). The Gibbs free energies of *OO, *OOH, *O, *OH, *H_2O_2, *OH-*OH and *OH on the surface of Pt doped Co_3O_4/EW-GQD, Co_3O_4/EW-GQD and Co_3O_4 were evaluated by using DFT calculations. The Gibbs free energy diagram for oxidase and peroxide-like was constructed by calculating the change in Gibbs free energy (ΔG) for each basic reaction step at 25°C. ΔG was calculated by subtracting the Gibbs free energy of the reactant from the product. The form is as follows: $\Delta G=\Delta E-T\Delta S$, where T is the absolute temperature, S is the entropy, and E is the energy. The adsorption energy of different catalyst for •OH were calcuated by following equation: $E_{ads,\bullet OH} = E_{\bullet OH@catalyst}-E_{catalyst}- E_{\bullet OH}$, where $E_{\bullet OH@catalyst}$ was the total energy of catalyst with an adsorbed hydroxyl, $E_{catalyst}$, and $E_{\bullet OH}$ were the total energies of catalyst and one free hydroxyl radical, respectively.

1.7. Total organic carbon test

The ability of Pt/Co/Co_3O_4/EW-GQD to mineralize Rhodamine B was determined by monitoring the change of total organic carbon (TOC) content under different reaction times during Rhodamine B degradation. The TOC removal efficiency is calculated by the following formula.

$$TOC\ Removal\ Efficiency\ (\%) = \frac{TOC_0 - TOC_t}{TOC_0} \times 100\% \qquad (4)$$

where, TOC_0 is the TOC value of the initial concentration of reaction solution and TOC_t is the TOC value of the reaction solution at different time.

2. Results and discussion

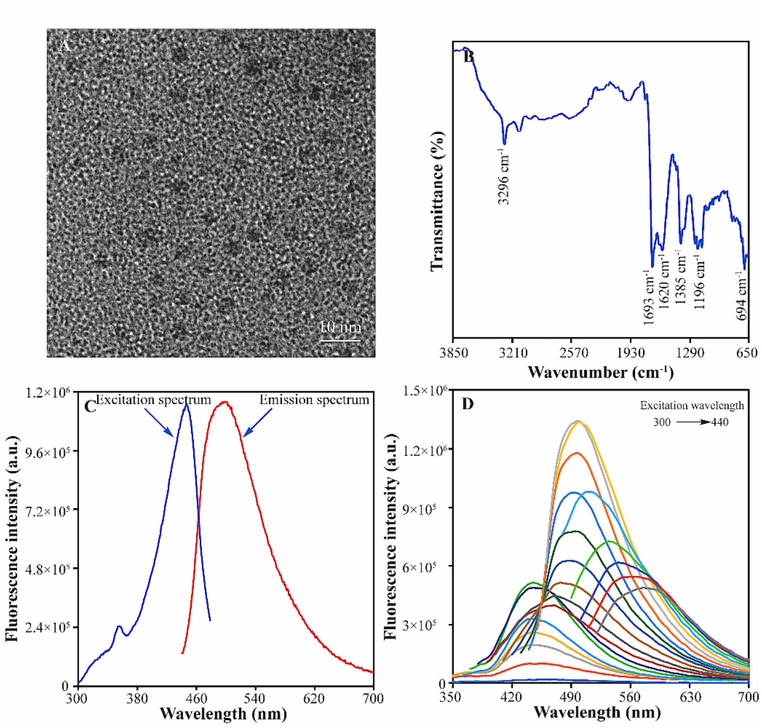

Fig. s1 TEM (A), FT-IR (B), excitation spectrum and emission spectrum (C) of EW-GQD and the emission specta (D) of EW-GQD at different excitation wavelengths.

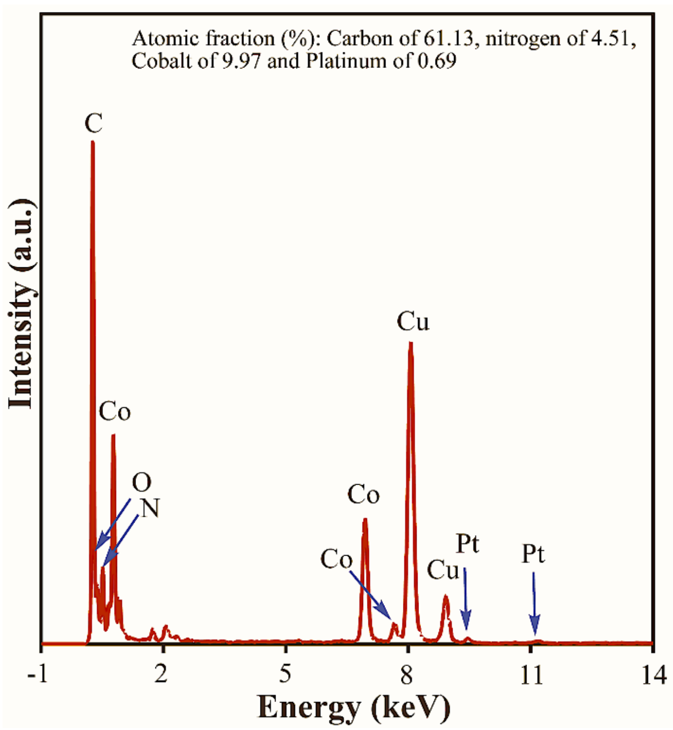

Fig. s2 EDS spectrum of $Pt/Co/Co_3O_4$/EW-GQD.

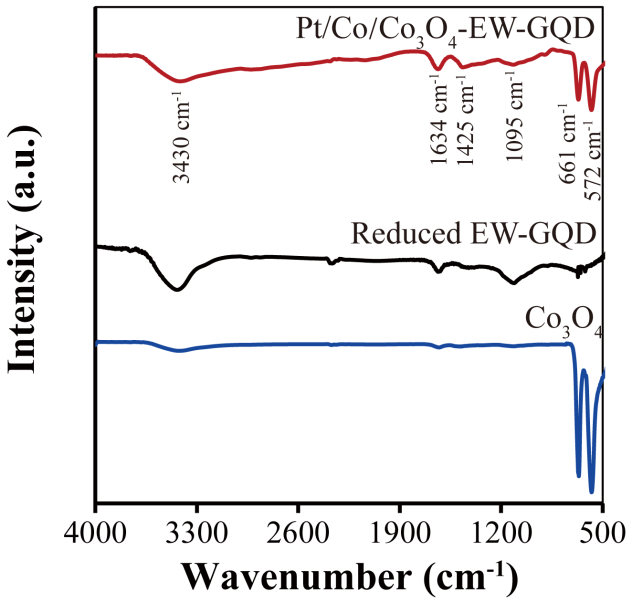

Fig. s3 FTIR spectra (A) of $Pt/Co/Co_3O_4$/EW-GQD, reduced EW-GQD and Co_3O_4.

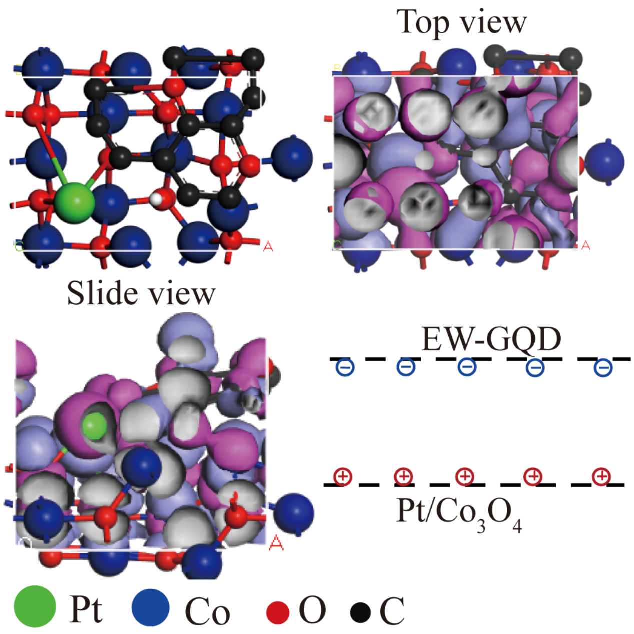

Fig. s4 Charge density difference maps of heterojunction combined by EW-GQD and $Pt/Co/Co_3O_4$. The blue and pink iso-surfaces represent gain and loss of electrons respectively

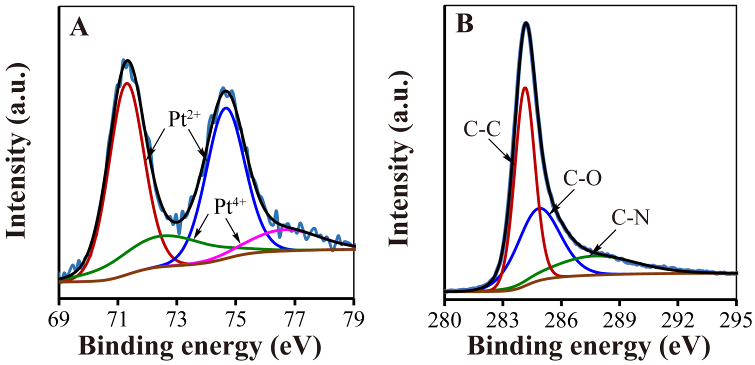

Fig. s5 High-resolution Pt4f (A) and C1s (B) XPS spectra of $Pt/Co/Co_3O_4$/EW-GQD.

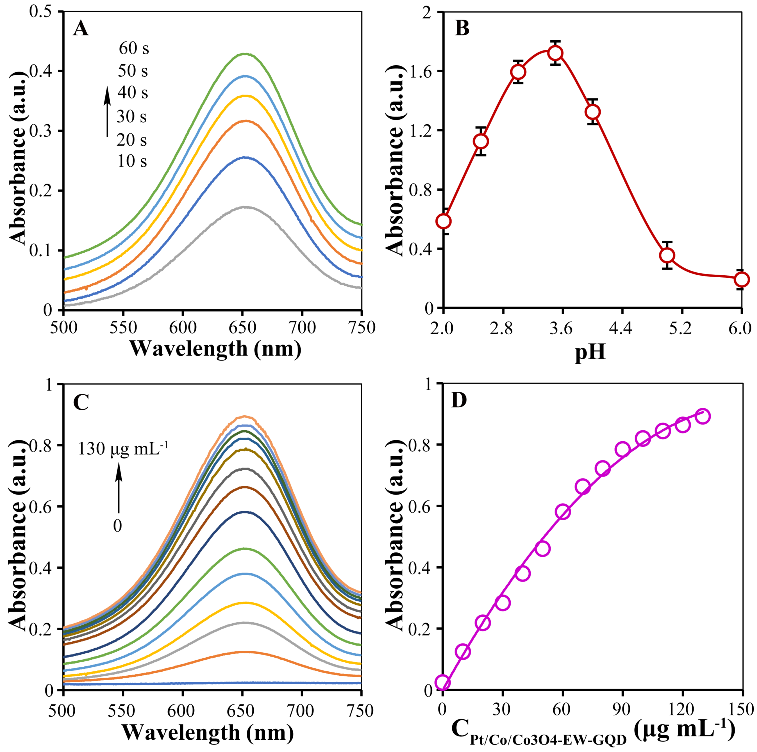

Fig. s6 Absorption spectra (A) of $Pt/Co/Co_3O_4$/EW-GQD+TMB under different catalyst concentrations ($Pt/Co/Co_3O_4$/EW-GQD concentration from bottom to top is 10, 20, 30, 40, 50, 60, 70, 80, 90, 100, 110, 120, 130 μg mL^{-1}); the relationship curve (B) between absorbance at 652 nm and $Pt/Co/Co_3O_4$/EW-GQD concentration; the relationship curve between absorbance at 652 nm and incubation time of the reaction system at a concentration of 100 μg mL^{-1}; the relationship curve between pH and the absorbance at 652nm of $Pt/Co/Co_3O_4$/EW-GQD+TMB.

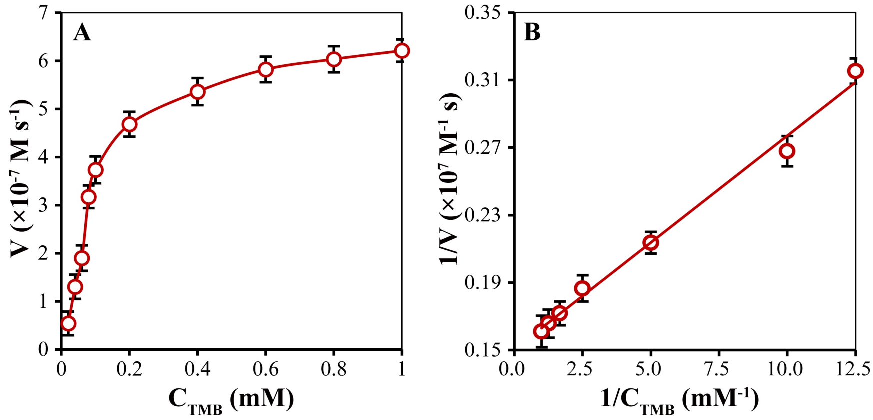

Fig. s7 Steady-state kinetic assay (A) and Lineweaver–Burk plot (B) for TMB of Co/Co_3O_4/EW-GQD.

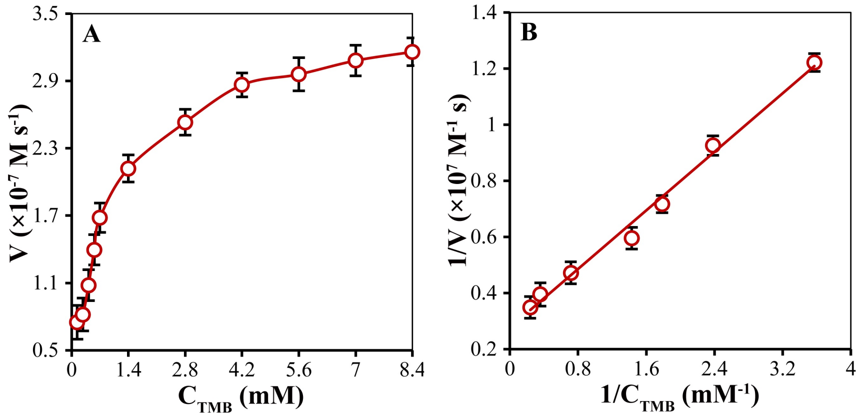

Fig. s8 Steady-state kinetic assay (A) and Lineweaver–Burk plot (B) for TMB of Co/Co_3O_4.

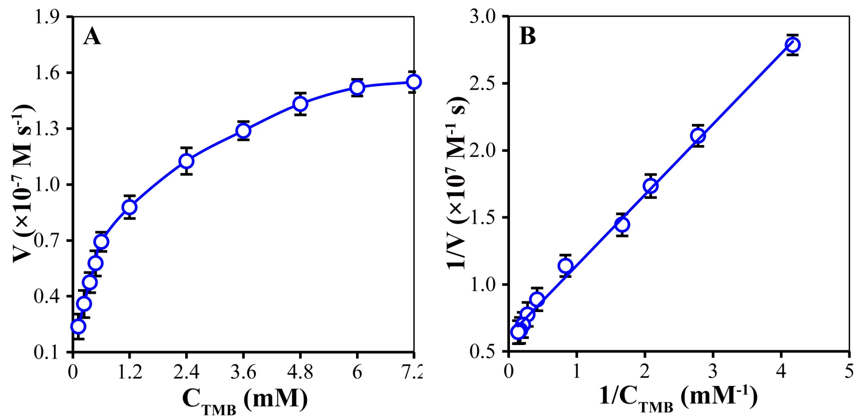

Fig. s9 Steady-state kinetic assay (A) and Lineweaver–Burk plot (B) for TMB of Co_3O_4.

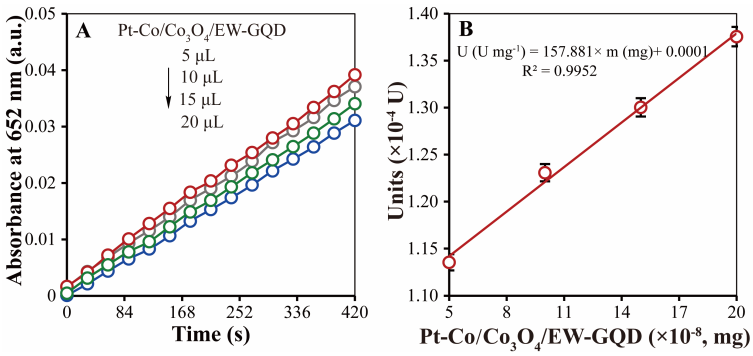

Fig. s10 Plots of the TMB reaction solutions added 5, 10, 15 and 20 μL of 10 ng mL^{-1} Pt/Co/Co_3O_4/EW-GQD vs. the incubation time (A), and relationship curve of oxidase-like activity (U mg^{-1}) with the amounts of Pt/Co/Co_3O_4/EW-GQD in the TMB reaction solution (B).

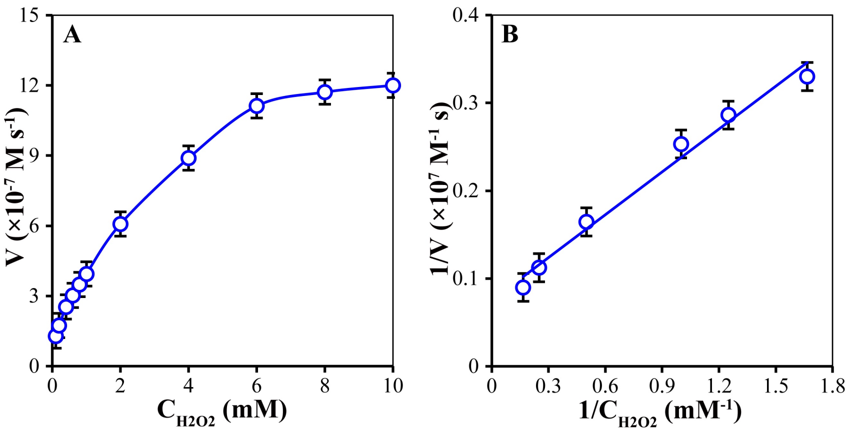

Fig. s11 Steady-state kinetic assay (A) and Lineweaver–Burk plot (B) for H_2O_2 of Pt/Co/Co_3O_4/EW-GQD.

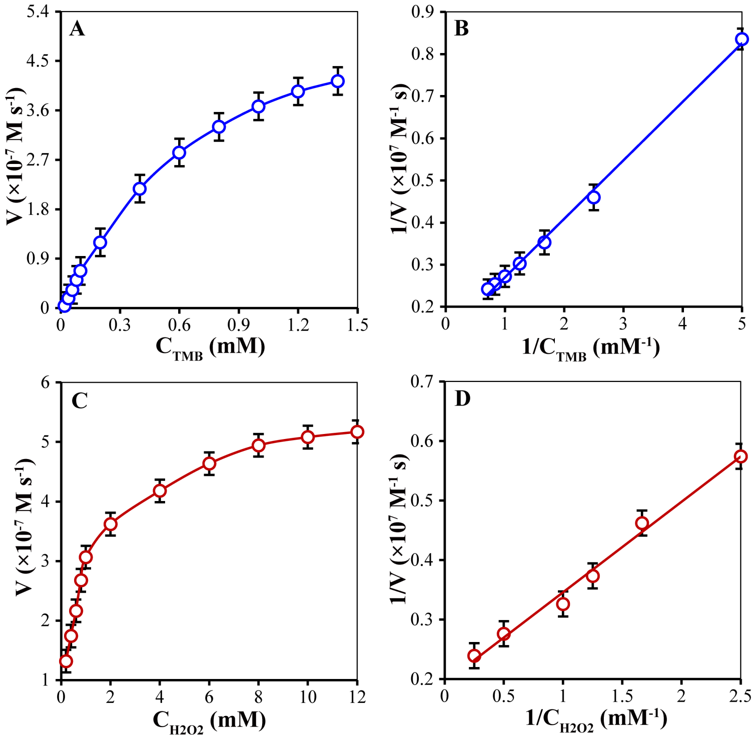

Fig. s12 Steady-state kinetic assay (A and C) and Lineweaver–Burk plot (B and D) for TMB and H_2O_2 of Co/Co_3O_4/EW-GQD

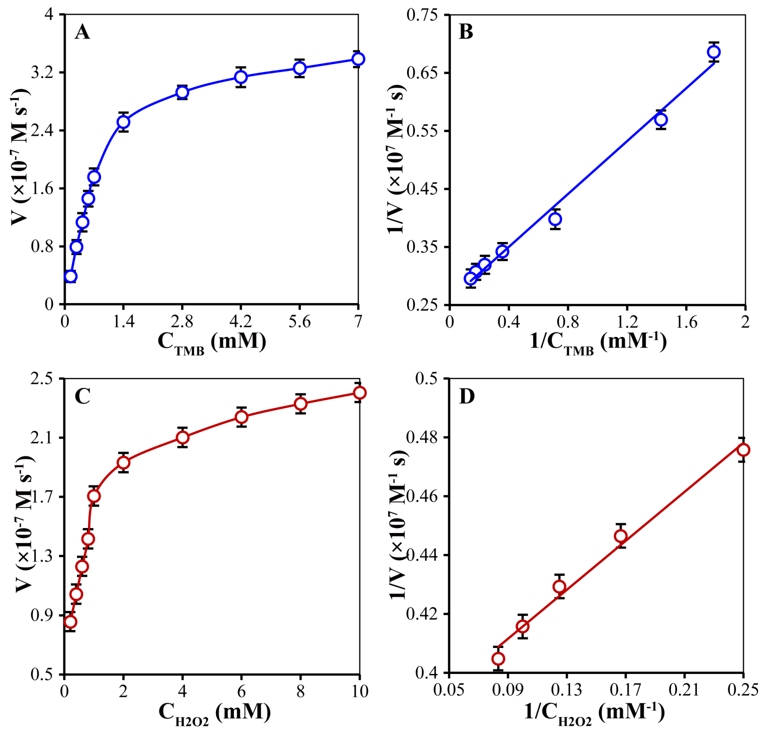

Fig. s13 Steady-state kinetic assay (A and C) and Lineweaver–Burk plot (B and D) for TMB and H_2O_2 of Co/Co_3O_4.

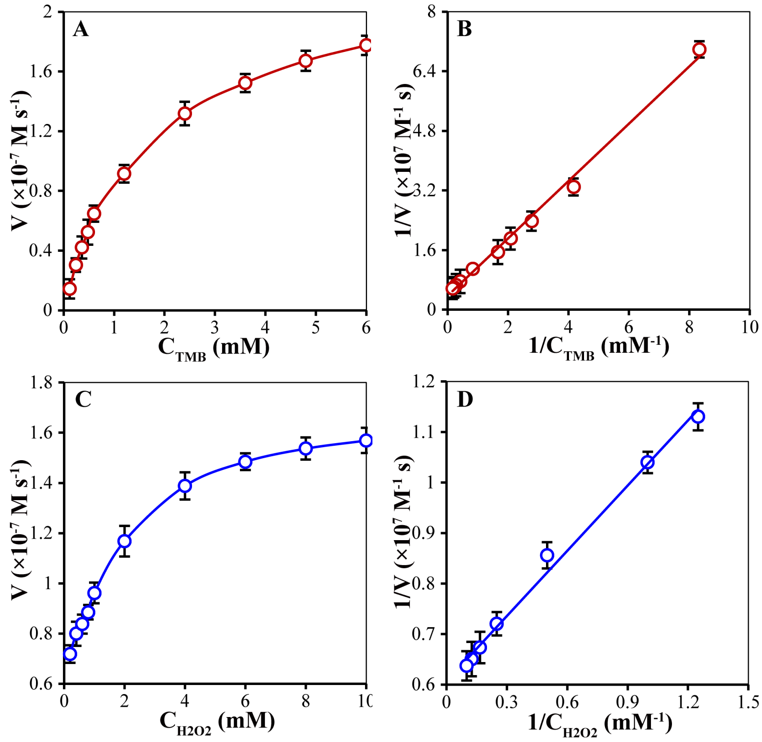

Fig. s14 Steady-state kinetic assay (A and C) and Lineweaver–Burk plot (B and D) for TMB and H_2O_2 of Co_3O_4.

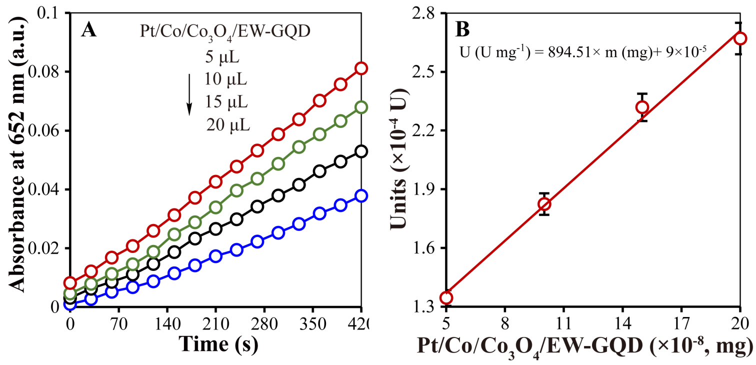

Fig. s15 Plots of the TMB reaction solutions added 5, 10, 15 and 20 μL of 10 ng mL^{-1} Pt/Co/Co_3O_4/EW-GQD vs. the incubation time (A), and relationship curve of peroxidase-like activity (U mg^{-1}) with the amounts of Pt/Co/Co_3O_4/EW-GQD in the TMB reaction solution (B).

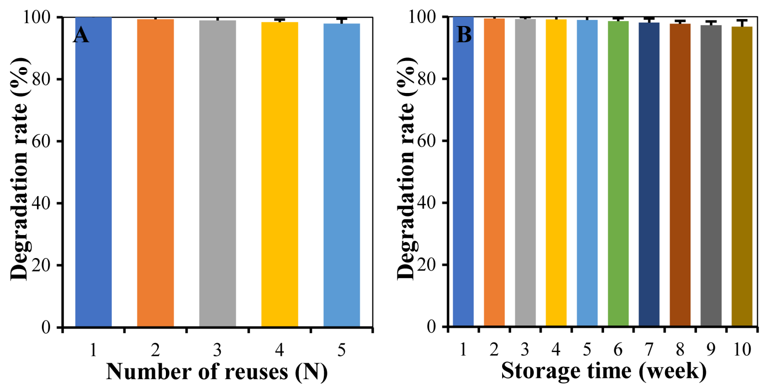

Fig. s16 Degradation efficiencies of 5 min incubation in the presence of 0.6 mg mL^{-1} Pt/Co/Co_3O_4/EW-GQD with different number of reuses (E), and degradation efficiencies of Rhodamine B in the presence of 0.6 mg mL^{-1} Pt/Co/Co_3O_4/EW-GQD with different standing time (F).

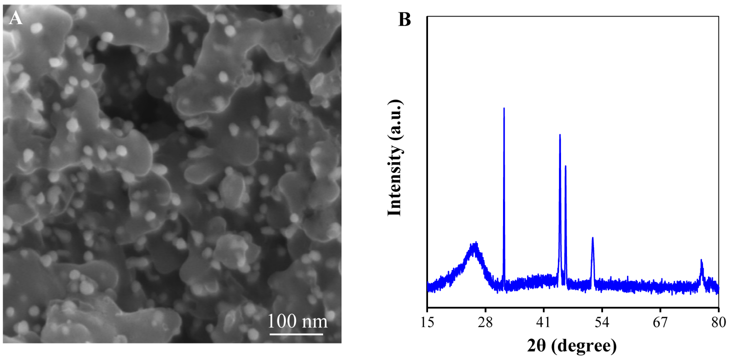

Fig. s17 SEM and XRD pattern of Pt/Co/Co_3O_4/EW-GQD after 5 cycles of use

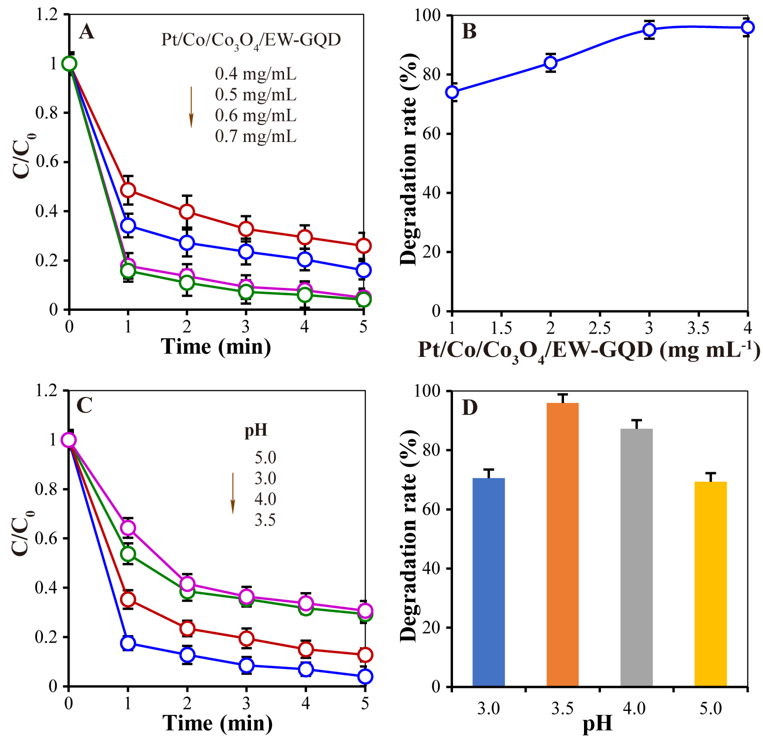

Fig. s18 Plots (A) of C/C_0 vs. the incubation time and degradation efficiencies (B) of 5 min incubation with 0.4, 0.5, 0.6 and 0.7 mg mL^{-1} Pt/Co/Co_3O_4/EW-GQD, plots (C) of C/C_0 vs. the incubation time and degradation efficiencies (D) of 5 min incubation in the pH of 3.0, 3.5, 4.0 and 5.0.

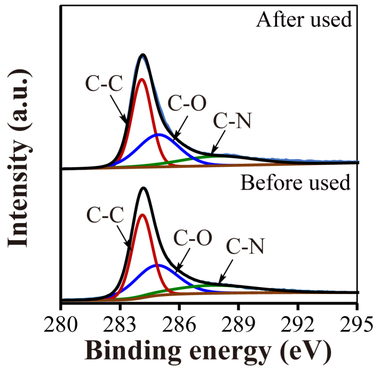

Fig. s19 High-resolution XPS spectra of C1s of $Pt/Co/Co_3O_4$/EW-GQD nanozyme before and after used

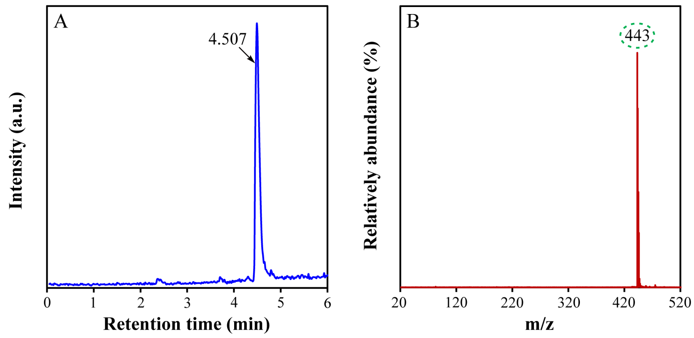

Fig. s20 High performance liquid chromatography (A) and mass spectra (B) of RhB before degradation

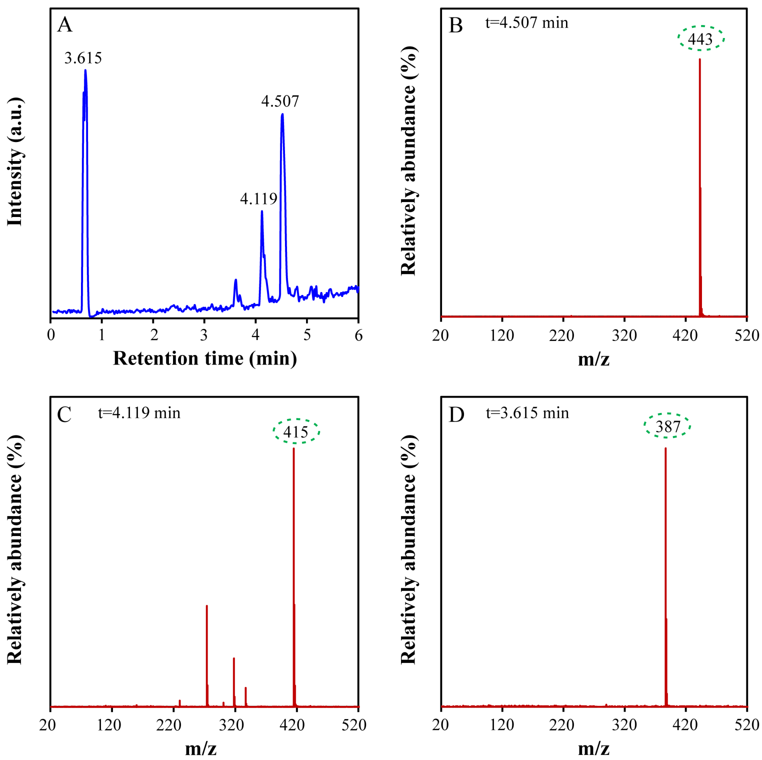

Fig. s21 High performance liquid chromatography (A) and mass spectra (B-D) of RhB degradation products after degradation time of 0.5 min

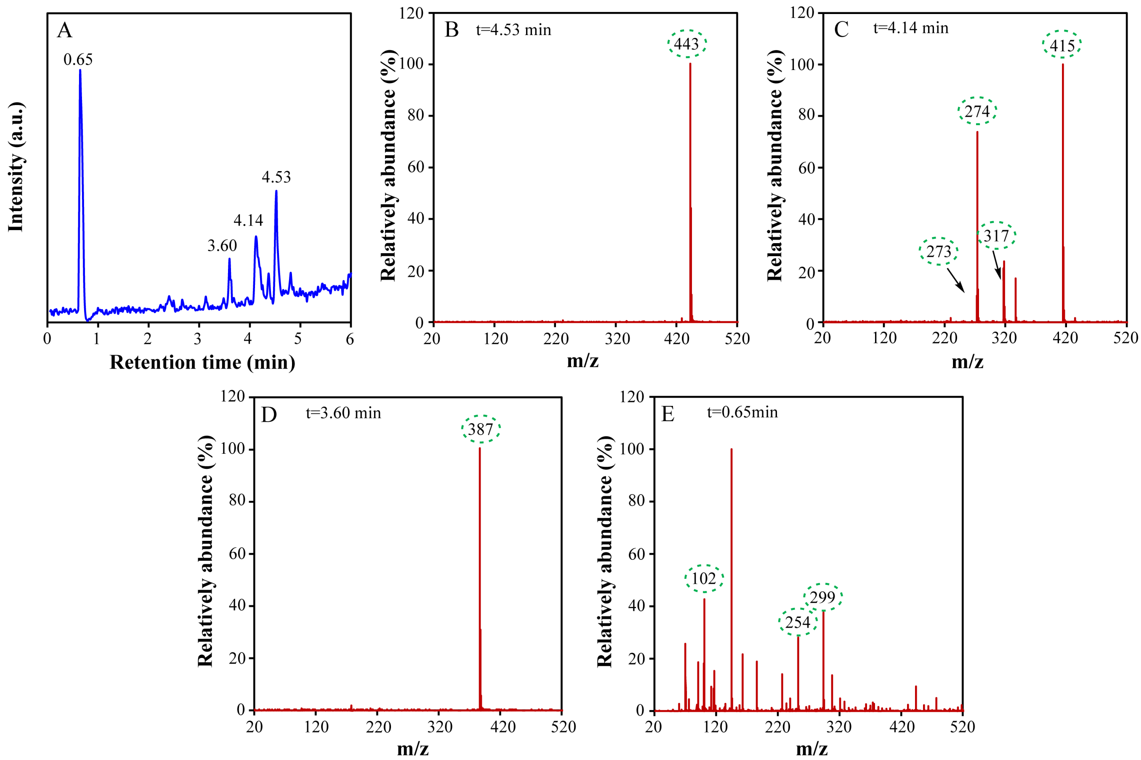

Fig. s22 High performance liquid chromatography (A) and mass spectra (B-E) of RhB degradation products after degradation time of 1 min

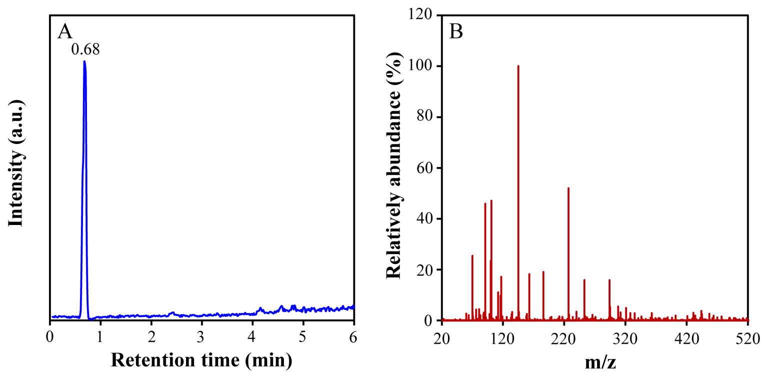

Fig. s23 High performance liquid chromatography (A) and mass spectra (B) of RhB degradation products after degradation time of 5 min

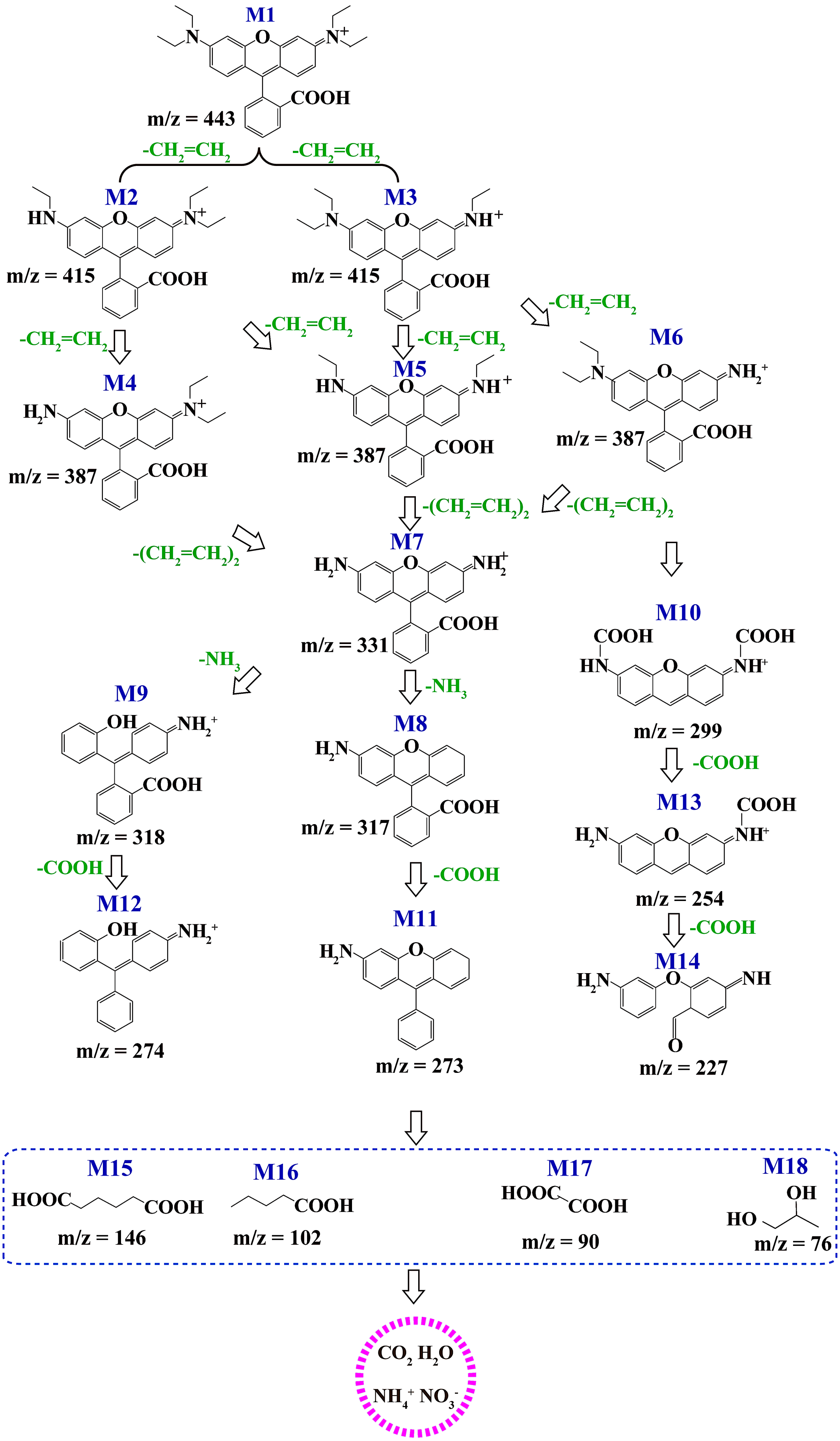

Fig. 24 Possible degradation pathway of Rhodamine B

Table s1 Impedance parameters of different materials modified ITO glass calculated according to equivalent circuit

Electrode materials	R_s (Ω)	R_{ct} (Ω)
Co_3O_4	119.1	952.6
$Co@Co_3O_4$/EW-GQD	30.1	396.5
$Pt/Co@Co_3O_4$/EW-GQD	12.5	79.3

Table s2 Comparison of the kinetic parameters (K_M and V_{max}) of various oxidase-like nanozyme

Nanozymes	K_M (mM)	V_{max} (10^{-7} M s^{-1})	Ref.
Fe-N-C single-atom nanozymes	1.81	0.00601	6
Defect-rich graphene stabilized atomically dispersed Cu_3 clusters	2.98	1.15	7
Hollow C@MoS_2 nanotubes-Hg^{2+}	3.35	0.344	8
MoS_2-Hg^{2+}	5.23	0.159	8
ZIF-67 nanosheets	13.69	0.035	9
MOF-818 (Zr-Cu)	49.87	8.47	10
MOF-818 (Fe-Cu)	8.99	2.96	10
Mn_3O_4	5.1	0.092	11
CuO_2 nanodot-encapsulated metal-organic framework	5.29	0.11	12
Co_3O_4	0.85	1.62	**Present work**
$Co@Co_3O_4$	0.94	3.60	
$Co@Co_3O_4$/EW-GQD	0.54	5.54	
$Pt/Co@Co_3O_4$/EW-GQD	0.28	16.69	

Table s3 Comparison of the kinetic parameters (K_M and V_{max}) of various peroxidase-like nanozyme

Nanozymes	K_M (mM)		V_{max} (10^{-7} M s^{-1})		Ref.
	TMB		TMB	H_2O_2	
Fe single-atom nanozyme	3.92	0.243	5.88	8.25	13
ZIF-67 nanosheets	13.69	3.52	0.035	0.028	14
Cu-MOF	4.11	6.41	5.56	1.02	15
HRP	0.43	3.70	1	0.871	16
Mesoporous iron oxide	0.298	146.7	0.736	0.637	17

Pt clusters on the Fe single-atom nanozymes	1.8	19.6	14	16	18
Fe-Zr-MOL	1.24	0.22	0.91	0.39	19
Cu-N-C	3.76	19.94	7.505	2.007	20
Copper nanoclusters	1.125	5.1	0.72	1.68	21
Co_3O_4	2.10	0.71	2.73	1.65	**Present work**
$Co@Co_3O_4$	0.88	1.11	3.86	2.67	
$Co@Co_3O_4$/EW-GQD	0.77	0.78	8.31	5.16	
Pt/$Co@Co_3O_4$/EW-GQD	0.061	2.16	14.30	13.31	

Table s4 Comparison of catalytic activity of different nanozymes

Nanozyme	Enzyme-like activity	Specific activity ($U\ mg^{-1}$)	Temperature (°C)	Ref.
Fe-N-C single-atom nanozyme	Peroxidase-like	57.76	37	[22]
Citrate-Os NPs	Peroxidase-like	393	55	[23]
Citrate-Pt NPs	Peroxidase-like	323.7	55	[23]
Citrate-Au NPs	Peroxidase-like	1.35	55	[23]
Fe_2O_3/carbon nanotubes	Peroxidase-like	25.4	37	[24]
Cellulose nanofibrils-supported PdNPs	Peroxidase-like	0.415	30	[25]
	Oxidase-like	0.277	30	
Fe,N co-doped ultrathin hollow carbon framework	Peroxidase-like	36.6	40	[26]
N doped carbon	Peroxidase-like	6.3	40	[26]
Fe,N co-doped carbon	Peroxidase-like	15.2	40	[26]
PdNPs/ TEMPO-oxidized cellulose nanofibril	Peroxidase-like	0.215	30	[27]
	Oxidase-like	0.107	30	
Prussian blue nanoparticles	Peroxidase-like	465.8	37	[28]
Fe single-atom/Pt clusters	Peroxidase-like	87.7	37	[29]
AuPtCo	Peroxidase-like	27.1	Room temperature	[30]
Pyrite	Peroxidase-like	58	37	[31]
Pt/$Co@Co_3O_4$/EW-GQD	Peroxidase-like	1662.64	37	**This work**
	Oxidase-like	293.45	37	

Table s5 The proportion of key elements in different chemical states in fresh and used Pt/$Co@Co_3O_4$/EW-GQD

Elements	Chemical states	Content before used (%)	Content after used (%)	Change value after and before used (%)

C	C-C	38.91	46.31	7.40
	C-O	39.11	34.87	-4.24
	C-N	21.98	18.82	-3.16
N	pyrrole N	45.38	47.08	1.70
	pyridine N	35.59	32.27	-3.32
	graphite N	19.03	20.65	1.62
O	lattice oxygen	74.23	75.34	1.11
	oxygen vacancy	25.77	24.66	-1.11
Co	Co^0	50.53	54.98	4.45
	Co^{2+}	14.47	10.26	-4.21
	Co^{3+}	35.00	34.76	-0.24
Pt	Pt^{2+}	74.70	75.59	0.89
	Pt^{4+}	25.30	24.41	-0.89

Reference

1. Z. G. Khan, T. N. Agrawal, S. B. Bari, S. N. Nangare and P. O. Patil, Application of surface nitrogen-doped graphene quantum dots in the sensing of ferric ions and glutathione: Spectroscopic investigations and DFT calculations, Spectrochim. Acta A, 2024, 306, 123608.
https://doi.org/10.1016/j.saa.2023.123608.

2. B. Jiang, D. M. Duan, L. Z. Gao, M. J. Zhou, K. L. Fan, Y. Tang, J. Q. Xi, Y. H. Bi, Z. Tong, G. F. Gao, N. Xie, A. F. Tang, G. H. Nie, M. M. Liang and X. Y. Yan, Standardized assays for determining the catalytic activity and kinetics of peroxidase-like nanozymes, Nat. Protoc., 2018, 3, 1506-1520.
https://doi.org/10.1038/s41596-018-0001-1.

3. G. Kresse and J. Furthmüller, Efficiency of ab-initio total energy calculations for metals and semiconductors using a plane-wave basis set, Comp. Mater. Sci., 1996, 6, 15-50.
https://doi.org/10.1016/0927-0256(96)00008-0.

4. G. Kresse and J. Furthmüller, Efficient iterative schemes for ab initio total-energy calculations using a plane-wave basis set, Phys. Rev. B, 1996, 54, 11169-11186.
https://doi.org/10.1103/PhysRevB.54.11169.

5. J. P. Perdew, K. Burke and M. Ernzerhof, Generalized Gradient Approximation Made Simple, Phys. Rev. Lett., 1996, 77, 3865-3868.
https://doi.org/10.1103/PhysRevLett.77.3865.

6. Y. Wu, L. Jiao, X. Luo, W. Q. Xu, X. Q. Wei, H. J. Wang, H. Y. Yan, W. L. Gu, B. Z. Xu, D. Du, Y. H. Lin and C. Z. Zhu, Oxidase-Like Fe-N-C Single-Atom Nanozymes for the Detection of Acetylcholinesterase Activity, Small, 2019, 15, 1903108.

https://doi.org/10.1002/smll.201903108.

7. F. C. Meng, M. Peng, Y. L. Chen, X. B. Cai, F. Huang, L. N. Yang, X. Liu, T. Li, X. D. Wen, N. Wang, D. Q. Xiao, H. Jiang, L. X. Xia, H. Y. Liu and D. Ma, Defect-rich graphene stabilized atomically dispersed Cu-3 clusters with enhanced oxidase-like activity for antibacterial applications, Appl. Catal. B: Environ., 2022, 301, 120836.

https://doi.org/10.1016/j.apcatb.2021.120826.

8. L. P. Feng, L. X. Zhang, Y. S. Gong, Z. L. Du, X. Chen, X. Y. Qi, X. Q. Zhang, G. J. Mao, H. Wang, Hollow C@MoS_2 nanotubes with Hg^{2+}-triggered oxidase-like catalysis: A colorimetric method for detection of Hg^{2+} ions in wastewater, Sensor. Actuat. B: Chem., 2022, 361 () 131725.

https://doi.org/10.1016/j.snb.2022.131725.

9. S. J. Wang, D. P. Xu, L. Ma, J. X. Qiu, X. Wang, Q. L. Dong, Q. Zhang, J. Pan and Q. Liu, Ultrathin ZIF-67 nanosheets as a colorimetric biosensing platform for peroxidase-like catalysis, Anal. Bioanal. Chem., 2018, 410, 7145-7152.

https://doi.org/10.1007/s00216-018-1317-y.

10. S. Kulandaivel, C. H. Lin and Y. C. Yeh, The bi-metallic MOF-919 (Fe-Cu) nanozyme capable of bifunctional enzyme-mimicking catalytic activity, Chem. Commun., 2022, 58, 569-572.

https://doi.org/10.1039/d1cc05908d.

11. Y. R. Chen, Y. D. Xia, Y. W. Liu, Y. Tang, F. Q. Zhao and B. Z. Zeng, Colorimetric and electrochemical detection platforms for tetracycline based on surface molecularly imprinted polyionic liquid on Mn_3O_4 nanozyme, Biosens. Bioelectron., 2022, 216, 114650.

https://doi.org/10.1016/j.bios.2022.114650.

12. W. H. Wang, S. Xiao, M. L. Zeng, H. Z. Xie and N. Gan, Dual-mode colorimetric-electrochemical biosensor for Vibrio parahaemolyticus detection based on CuO_2 nanodot-encapsulated metal-organic framework nanozymes, Sensor. Actuat. B: Chem., 2023, 387, 133835.

https://doi.org/10.1016/j.snb.2023.133835.

13. C. Zhao, C. Xiong, X. K. Liu, M. Qiao, Z. J. Li, T. W. Yuan, J. Wang, Y. T. Qu, X. Q. Wang, F. Y. Zhou, Q. Xu, S. Q. Wang, M. Chen, W. Y. Wang, Y. F. Li, T. Yao, Y. E. Wu and Y. D. Li, Unraveling the enzyme-like activity of heterogeneous single atom catalyst, Chem. Comm., 2019, 55, 2285-2288.

https://doi.org/10.1039/c9cc00199a.

14. S. J. Wang, D. P. Xu, L. Ma, J. X. Qiu, X. Wang, Q. L. Dong, Q. Zhang, J. Pan and Q. Liu, Ultrathin ZIF-67 nanosheets as a colorimetric biosensing platform for peroxidase-like catalysis, Anal. Bioanal. Chem., 2018, 410, 7145–7152.
https://doi.org/10.1007/s00216-018-1317-y.

15. C. H. Wang, J. Gao and H. L. Tan, Integrated Antibody with Catalytic Metal-Organic Framework for Colorimetric Immunoassay, ACS Appl. Mater. Interfaces, 2018, 10, 25113-25120.
https://doi.org/10.1021/acsami.8b07225.

16. M. M. Liang and X. Y. Yan, Nanozymes: From New Concepts, Mechanisms, and Standards to Applications, Acc. Chem. Res., 2019, 52, 2190-2200.
https://doi.org/10.1021/acs.accounts.9b00140.

17. R. Bhattacharjee, S. Tanaka, S. Moriam, M. Kamal Masud, J. J. Lin, S. M. Alshehri, T. Ahamad, R. R. Salunkhe, N. T. Nguyen, Y. Yamauchi, M. S. A. Hossain and M. J. A. Shiddiky, Porous nanozymes: the peroxidase-mimetic activity of mesoporous iron oxide for the colorimetric and electrochemical detection of global DNA methylation, J. Mater. Chem. B, 2018, 6, 4783-4791.
https://doi.org/10.1039/c8tb01132j.

18. Y. F. Chen, L. Jiao, H. Y. Yan, W. Q. Xu, Y. Wu, L. R. Zheng, W. L. Gu and C. Z. Zhu, Fe-N-C Single-Atom Catalyst Coupling with Pt Clusters Boosts Peroxidase-like Activity for Cascade-Amplified Colorimetric Immunoassay, Anal. Chem., 2021, 93, 12353-12359.
https://doi.org/10.1021/acs.analchem.1c02115.

19. Z. Wu, J. Wen, J. Li, L. Chen, W. Li and K. Yang, The engineering design of single-site nanozyme based on metal-organic layers for the detection of antioxidant substances, Mater. Today Chem., 2023, 30, 101598.
https://doi.org/10.1016/j.mtchem.2023.101598.

20. Y. Wu, J. B. Wu, L. Jiao, W. Q. Xu, H. J. Wang, X. Q. Wei, W. L. Gu, G. X. Ren, N. Zhang, Q. H. Zhang, L. Huang, L. Gu and C. Z. Zhu, Cascade Reaction System Integrating Single-Atom Nanozymes with Abundant Cu Sites for Enhanced Biosensing, Anal. Chem., 2020, 92, 3373-3379.
https://dx.doi.org/10.1021/acs.analchem.9b05437.

21. C. Y. Liu, Y. Y. Cai, J. Wang, X. Liu, H. Ren, L. Yan, Y. J. Zhang, S. Q. Yang, J. Guo and A. H. Liu, Facile Preparation of Homogeneous Copper Nanoclusters Exhibiting Excellent Tetraenzyme Mimetic Activities for Colorimetric Glutathione Sensing and Fluorimetric Ascorbic Acid Sensing, ACS Appl. Mater. Interfaces, 2020, 12, 42521-42530.
https://dx.doi.org/10.1021/acsami.0c11983.

22. X. H. Niu, Q. R. Shi, W. L. Zhu, D. Liu, H. Y. Tian, S. F. Fu, N. Cheng, S. Q. Li, J. N. Smith, D. Du and Y. H. Lin, Unprecedented peroxidase-mimicking activity of single-atom nanozyme with atomically dispersed Fe–N_x moieties hosted by MOF derived porous carbon, Biosens. Bioelectron., 2019, 142, 111495.

https://doi.org/10.1016/j.bios.2019.111495.

23. S. B. He, L. Yang, P. Balasubramanian, S. J. Li, H. P. Peng, Y. Kuang, H. H. Deng and W. Chen, Osmium nanozyme as peroxidase mimic with high performance and negligible interference of O_2, J. Mater. Chem. A, 2020, 8, 25226-25234.

https://doi.org/10.1039/d0ta09247a.

24. Y. C. Yang, T. Li, Y. Qin, L. B. Zhang and Y. Chen, Construct of Carbon Nanotube-Supported Fe_2O_3 Hybrid Nanozyme by Atomic Layer Deposition for Highly Efficient Dopamine Sensing, Front. Chem., 2020, 8, 564968.

https://doi.org/10.3389/fchem.2020.564968

25. R. Dadigala, R. Bandi, M. Alle, C. W. Park, S. Y. Han, G. J. Kwon and S. H. Lee, Effective fabrication of cellulose nanofibrils supported Pd nanoparticles as a novel nanozyme with peroxidase and oxidase-like activities for efficient dye degradation, J. Hazard. Mater., 2022, **436**, 129165.

https://doi.org/10.1016/j.jhazmat.2022.129165.

26. J. Y. Hao, C. Zhang, C. X. Feng, Q. Wang, Z. Y. Liu, Y. Li, J. S. Mu, E. C. Yang and Y. Wang, An ultra-highly active nanozyme of Fe,N co-doped ultrathin hollow carbon framework for antibacterial application, Chinese Chem. Lett., 2023, 34, 107650.

https://doi.org/10.1016/j.cclet.2022.06.073.

27. R. Dadigala, R. Bandi, S. Y. Han, G. J. Kwon and S. H. Lee, Rapid in-situ growth of enzyme-mimicking Pd nanoparticles on TEMPO-oxidized nanocellulose for the efficient detection of ascorbic acid, Int. J. Biol. Macromol., 2023, 234, 123657.

https://doi.org/10.1016/j.ijbiomac.2023.123657.

28. Z. G. Qin, B. Chen, Y. Mao, C. Shi, Y. Li, X. Huang, F. Yang and N. Gu, Achieving Ultrasmall Prussian Blue Nanoparticles as HighPerformance Biomedical Agents with Multifunctions, ACS Appl. Mater. Interfaces, 2020, 12, 57382-57390.

https://dx.doi.org/10.1021/acsami.0c18357.

29. Y. F. Chen, L. Jiao, H. Y. Yan, W. Q. Xu, Y. Wu, L. R. Zheng, W. L. Gu and C. Z. Zhu, Fe−N−C Single-Atom Catalyst Coupling with Pt Clusters Boosts Peroxidase-like Activity for Cascade-Amplified Colorimetric Immunoassay, Anal. Chem., 2021, 93, 12353-12359.

https://doi.org/10.1021/acs.analchem.1c02115.

30. X. Y. Zhou, C. Fan, Q. W. Tian, C. H. Han, Z. Q. Yin, Z. Y. Dong and S. Bi, Trimetallic AuPtCo Nanopolyhedrons with Peroxidase- and Catalase-Like Catalytic Activity for Glow-Type Chemiluminescence Bioanalysis, Anal. Chem., 2022, 94, 847-855.

https://doi.org/10.1021/acs.analchem.1c03572.

31. X. Q. Meng, D. D. Li, L. Chen, H. L. He, Q. Wang, C. Y. Hong, J. Y. He, X. F. Gao, Y. L. Yang, B. Jiang, G. H. Nie, X. Y. Yan, L. Z. Gao and K. L. Fan, High-Performance Self-Cascade Pyrite Nanozymes for Apoptosis−Ferroptosis Synergistic Tumor Therapy, ACS Nano, 2021, 15, 5735-5751.

https://dx.doi.org/10.1021/acsnano.1c01248.